PHYSICAL REVIEW VOLUME 161, NUMBER 3 15 SEPTEMBER 1967

# Tunneling Spectroscopy in GaAs

J. W. CONLEY AND G. D. MAHAN

*General Electric Research and Development Center, Schenectady, New York*

(Received 7 November 1966; revised manuscript received 28 February 1967)

Observations of tunneling in Schottky barriers made from $n$- and $p$-type GaAs with Au as the metallic element are presented in detail. The characteristics are expressed in terms of the dependence of incremental resistance $dV/dI$ on applied voltage $V$. These are interpreted in terms of a theory which uses the WKBJ approximations and a two-band formulation for the dispersion of states of the forbidden gap. An experimental determination of this dispersion is made which proves to be consistent with the theory. In this determination, a technique is introduced in which the characteristics are measured directly as $d\ln I/dV$. Fine structure is observed superposed on the background characteristic at $\pm\hbar\omega_0$ and is interpreted as a many-body polar (polaron) interaction. Some new aspects of the problem of zero-bias anomalies are presented.

## I. INTRODUCTION

TUNNELING experiments are capable of providing useful information about the properties of semiconductors. The Schottky barrier formed at a metal-semiconductor interface constitutes a junction with a simple and well-understood space-charge region.[1,2] Tunneling experiments in this system can be analyzed relatively easily.[3–5] This allows one to determine the important physical processes involved in tunneling, and also to deduce information on the properties of the semiconductor. This is in contrast with $p$-$n$ junctions which have a more complicated space-charge region, and are more difficult to analyze. Another advantage of Schottky barriers is that $n$- and $p$-type semiconductors can be studied separately.

The present article reports Schottky tunneling measurements of the metal Au on both $n$- and $p$-type GaAs. GaAs was selected for the present study because its properties are relatively well known and metal-semiconductor contacts can be formed easily. A description of the junction fabrication and electrical measurements are given in Sec. IV. Previous information already exists for the values of the conduction band mass[6] $m_c=0.072$, dielectric constant $\epsilon_0=13$, low-temperature gap[7] $E_g=1.52$ eV, and barrier heights $V_B=0.92$ eV for $n$-type and $V_B=0.46$ eV for $p$-type. Our dispersion measurements on $p$-type GaAs show that light holes do the tunneling, and provide a measurement of the light-hole mass.

The previous calculations of Conley, Duke, Mahan, and Tiemann[3] (CDMT) showed that the incremental resistance measurements ($dV/dI$) of $n$-type Ge would have maxima at biases equal to the Fermi degeneracy of the conduction band. This has been verified experimentally by Conley and Tiemann.[5] This behavior arises because the Fermi energy is small due to the many-valley structure of $n$-type Ge, and electrons from the bottom of the band can tunnel nearly as readily as those at the Fermi energy. The maximum occurs at biases equal to the Fermi energy because of the discontinuity in the density of states at the bottom of the band. Band tailing is thought to be observed in the smearing of this maximum.

Degenerate $p$-type semiconductors also have small Fermi energies because the heavy hole dominates the density-of-states mass. The tunneling characteristics of $p$-type GaAs are quite similar to those for $n$-type Ge. The theory of CDMT also describes the incremental resistance data for this material. It is not possible to deduce the Fermi degeneracy from the position of the resistance maximum because band tailing is particularly severe. The heavy hole causes the impurity band to be much deeper into the forbidden gap in $p$-type materials. In another communication,[8] we have shown how the $p$-type GaAs data can be reduced to provide a measurement of the impurity band.

In $n$-type GaAs, the Fermi energies are large since the density-of-states mass is small. Electrons at the bottom of the band are shown to be unimportant in the tunneling process. Thus, the incremental resistance does not peak at a bias equal to the Fermi degeneracy, but at a much smaller value. Here the most important effect for determining the junction resistance characteristics is the band mixing in the forbidden gap. Since $V_B/E_G=\frac{2}{3}$,[9] the electron tunneling in the forbidden energy gap has acquired a considerable valence-band character before encountering the metallic surface.[4]

[1] H. K. Henisch, *Rectifying Semiconductor Contacts* (Clarendon Press, Ltd., Oxford, England, 1957).
[2] B. R. Gossick, *Potential Barriers in Semiconductors* (Academic Press Inc., New York, 1964).
[3] J. W. Conley, C. B. Duke, G. D. Mahan, and J. J. Tiemann, Phys. Rev. **150**, 466 (1966).
[4] F. A. Padovani and R. Stratton, Phys. Rev. Letters **16**, 1202 (1966); G. Lewicki and C. A. Mead, *ibid.* **16**, 939 (1966).
[5] J. W. Conley and J. J. Tiemann, J. Appl. Phys. **38**, 2880 (1967).
[6] H. Ehrenreich, Phys. Rev. **120**, 1951 (1960); T. S. Moss and A. K. Walton, Proc. Phys. Soc. (London) **74**, 131 (1959); M. Cardona, Phys. Rev. **121**, 752 (1961); W. G. Spitzer and J. M. Whelan, Phys. Rev. **114**, 59 (1959); Yu. I. Ukanhov, Fiz. Tver. Tela. **5**, 108 (1963) [English transl.: Soviet Phys.—Solid State **5**, 75 (1963)]; E. D. Palik, S. Teitler, and R. F. Wallis, J. Appl. Phys. **32**, 2132 (1961).
[7] M. D. Sturge, Phys. Rev. **127**, 768 (1962).
[8] G. D. Mahan and J. W. Conley, Appl. Phys. Letters (to be published).
[9] C. A. Mead and W. G. Spitzer, Phys. Rev. **134**, A713 (1964). The barrier heights of 0.92 and 0.46 eV are typical values from these data. Also see D. V. Geppert, A. M. Cowley, and B. V. Dore, J. Appl. Phys. **37**, 2458 (1966).

This behavior can be calculated by adopting a two-band model.[10,11] The WKBJ trajectory we use to evaluate the current in the metal-semiconductor junction is a simple extension of that used for *p-n* diodes by Butcher, Hulbert, and Hulme.[12] The incremental resistance calculated using these WKBJ integrals agree satisfactorily with experiment. Band-mixing effects are unimportant in *n*-type Ge or *p*-type GaAs since $V_B/E_G<\frac{1}{2}$ and the amount of mixing which occurs is negligible.

Padovani and Stratton[4] have also recently described metal-semiconductor tunneling in *n*-type GaAs in terms of a two-band model. They suggested a method which expresses the dispersion $k^2(E)<0$ for electron states in the forbidden gap in terms of $d\ln I/dV$. Their results, obtained by numerical differentiation of the $V(I)$ characterization, disagree with the prediction of $\mathbf{k}\cdot\mathbf{p}$ perturbation theory for the two-band model. Our results obtained through direct measurement of $d\ln I/dV$ are given in Sec. VI. We find agreement with the $\mathbf{k}\cdot\mathbf{p}$ theory for both *n*- and *p*-type GaAs. Further, this demonstrates that the light holes are responsible for the tunneling in *p*-type GaAs, and verifies the prediction of their effective mass from $\mathbf{k}\cdot\mathbf{p}$ theory.[6]

Mathematical aspects of several features of the potential barrier are discussed in Sec. II. The effect of a random distribution of impurities in the depletion region is discussed in Appendix A. This leads to fluctuations in the barrier potential which are as large as 0.1 eV. The effect on the tunneling characteristics of the departure from the parabolic dependence of a uniformly doped semiconductor in the reverse region is demonstrated in Appendix B.

Besides these one-electron effects, many-body effects are also observed in the resistance measurements. Zero-bias anomalies[13–18] are much stronger in *p*-type data than in *n*-type data. Other structure[13] occurs at biases $\pm\hbar\omega_0$, where $\omega_0$ is the LO phonon frequency. These are due to polaron effects, and are discussed extensively in Sec. VII. It is shown that the observed anomalies are caused by polaron alterations of the WKBJ exponents rather than density-of-states effects. The magnitude of the observed anomalies agrees with recent predictions of many-body theory.[19,20]

## II. BARRIER POTENTIALS

When an electron in the semiconductor enters the depletion region, the potential is, on the average, parabolic. The parabolicity is obtained by assuming that the impurity charge density $n_0$ is spread uniformly throughout the semiconductor. Then Poisson's equation is

$$\frac{\partial^2}{\partial z^2}V(z)=\frac{4\pi e^2 n_0}{\epsilon_0},$$

which gives the solution

$$V(z)=\frac{2\pi e^2 n_0}{\epsilon_0}(z-z_1)^2+V_1. \tag{2.1}$$

The constant $z_1$, the bottom of the parabola, is a constant of integration. The other constant $V_1$ will be chosen to make the potential zero at the bottom of the conduction band. The potential $V(z)$ ceases to be parabolic in the region where the conduction-electron density $n_e$ becomes appreciable. This effect can be estimated by assuming that the conduction electrons are a classical charge distribution of density

$$n_e(z)=\frac{k_F(z)^3}{3\pi^2}=\frac{(2m)^{3/2}}{3\pi^2}[\mu_F-V(z)]^{3/2}. \tag{2.2}$$

In the region where $n_e(z)$ is nonzero, Poisson's equation

$$\frac{\partial^2}{\partial z^2}V(z)=\frac{4\pi e^2}{\epsilon_0}[n_0-n_e(z)]. \tag{2.3}$$

These equations have already been solved for *p-n* junctions.[21–23] The solution for the Schottky barrier is even simpler. At zero temperature, the result is expressed as a single quadrature

$$V_p(z)=\frac{2\pi e^2 n_0}{\epsilon_0}(z-z_1)^2+\tfrac{2}{5}\mu_F \qquad z_0\geq z\geq 0,$$

$$k_s(z-z_0)=\frac{\sqrt{5}}{2}\int_0^{1-V(z)/\mu_F}\frac{d\lambda}{[1-(5/3)\lambda+\frac{2}{3}\lambda^{5/2}]^{1/2}} \qquad z>z_0, \tag{2.4a}$$

$$z_1=\left[\frac{\epsilon_0}{2\pi e^2 n_0}(V_B-V+3\mu_F/5)\right]^{1/2}, \qquad z_0=z_1-(3/\sqrt{5})k_s^{-1}, \tag{2.4b}$$

---

[10] W. Franz, in *Handbuch der Physik*, edited by S. Flügge, (Springer-Verlag, Berlin, 1956), Vol. XVIII, p. 155.
[11] E. O. Kane, J. Phys. Chem. Solids **1**, 249 (1957); **12**, 181 (1959).
[12] P. N. Butcher, J. A. Hulbert, and K. F. Hulme, J. Phys. Chem. Solids **21**, 320 (1961).
[13] R. N. Hall, J. H. Racette, and H. Ehrenreich, Phys. Rev. Letters **4**, 456 (1960); R. N. Hall and J. H. Racette, J. Appl. Phys. **32**, 2078 (1961); R. N. Hall, in *Proceedings of the International Conference on Semiconductor Physics, Prague, 1960* (Publishing House of the Czechoslovak Academy of Sciences, Prague, 1961), p. 163.
[14] A. F. G. Wyatt, Phys. Rev. Letters **13**, 401 (1964).
[15] R. A. Logan and J. M. Rowell, Phys. Rev. Letters **13**, 404 (1966); J. Shewchun and R. M. Williams, *ibid.* **15**, 160 (1965).
[16] J. M. Rowell and L. Y. L. Shen, Phys. Rev. Letters **17**, 15 (1966).
[17] J. Appelbaum, Phys. Rev. Letters **17**, 91 (1966).
[18] P. W. Anderson, Phys. Rev. Letters **17**, 95 (1966).
[19] S. Englesberg and J. R. Schrieffer, Phys. Rev. **131**, 993 (1963).
[20] G. D. Mahan and C. B. Duke, Phys. Rev. **149**, 705 (1966).
[21] I. I. Ivanchik, Fiz. Tver. Tela. **3**, 103 (1961) [English transl.: Soviet Phys.—Solid State **3**, 75 (1961)].
[22] P. Andres, in *Proceedings of the International Conference on the Physics of Semiconductors* (Dunod Cie., Paris, 1964), p. 593.
[23] D. J. BenDaniel and C. B. Duke, Phys. Rev. **152**, 683 (1966).

where $k_s$ in the Fermi-Thomas screening wave vector

$$k_s^2 = 6\pi n_0 e^2/\epsilon_0\mu_F.$$

These solutions are plotted in Fig. 1. By measuring distances in $k_s^{-1}$, and energies in $\mu_F$, this is a universal curve applicable to all junctions. The parabolic solution, valid for $z<z_0$, has its minimum $\frac{2}{5}\mu_F$ above the bottom of the conduction band. Also plotted in Fig. 1 is the exponential potential

$$V_e(z) = \mu_F \exp[-k_s(z-z_0)] \qquad z>z_0.$$

It is easy to show that the potential $V(z)$ has the asymptotic form $V_e(z)$ as $z\to\infty$. Further, the potential $V_e(z)$ approximates the exact solution reasonably well for all values $z>z_0$.

In the WKBJ calculations for the tunneling current, two types of potentials were used. The first is the exponential-parabolic form given above:

$$\begin{aligned} V_{ep}(z) &= V_e(z), \quad z>z_0 \\ &= V_p(z), \quad z_0 \geq z \geq 0. \end{aligned} \qquad (2.5)$$

The use of $V_e(z)$, rather than the exact solution (2.4b), allows the WKBJ integrals to be done analytically. The other potential is even a cruder approximation. Here it is assumed that the parabolic solution applies for all $z$, and the exponential character is ignored. Then the potential is

$$\begin{aligned} V_p'(z) &= \frac{2\pi e^2 n_0}{\epsilon_0}(z-z_2)^2, \quad z_2>z>0 \\ &= 0, \qquad\qquad z>z_2 \end{aligned} \qquad (2.6)$$

$$z_2 = \left[\frac{\epsilon_0}{2\pi n_0 e^2}(V_B - V + \mu_F)\right]^{1/2}.$$

The tunneling current predicted by these potentials are discussed in Appendix II. The differences are often slight, and then it is adequate to employ the simpler potential $V_p'$.

For the same set of parameters, the potential $V_{ep}$ always predicts a slightly wider space-charge region than $V_p'$. As shown below, this is the primary consequence of using the more accurate potential $V_{ep}$.

While in the junction, the electron feels its image force from the surface of the metal. Near the metal, this potential can be approximated as $-e^2/4\epsilon_0 z$. This is a small and negligible effect. At one lattice constant ($z\simeq 4$ Å) from the metal, the resulting 50 meV is small compared to the 1.0 eV of the surface barrier. The image potential was included in calculations using a WKBJ formalism. The integrals were evaluated using expansions similar to those of Stratton.[24] It was thereby determined that the small effect of the image potential on the tunneling current is nearly independent of voltage.

[24] R. Stratton, J. Phys. Chem. Solids **23**, 1177 (1962).

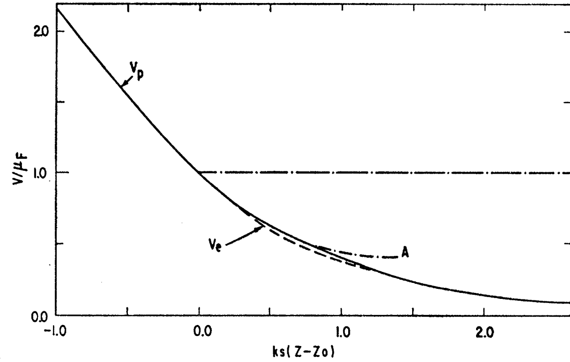


FIG. 1. The solid line is the potential $V(z)$ of an electron in the junction region. $V(z)$ is zero in the bulk semiconductor. The line $V=\mu_F$ indicates the Fermi degeneracy. For $z<z_0$, the conduction band is empty, and the potential is the parabolic form given in (2.4a). The minimum of this parabola is shown at the point $A$. For $z>z_0$, the solid line indicates the solution of (2.4b). Also shown is the exponential potential $V_e(z)$ which closely approximates the exact solution. By scaling energies to $\mu_F$ and distances to $k_s$, this is a universal curve applicable to all junctions. The parabolic solutions $V_p(z)$ ends at the surface $z=0$, and the value of $z_0$ is determined by the barrier height. The same curve applies to the valence band except that it is inverted.

The actual potential that an electron sees when entering a junction is not smooth as shown. If the impurity density is $10^{19}$ cm$^{-3}$, the impurity ions are, on the average, about 50 Å apart. The width of the depletion region is $\sim$100 Å. Thus, fluctuations in the density of the randomly located impurity ions will lead to appreciable effects. It is well known that this is the cause of band tailing.[25,26] In the tunneling problem, an additional consequence is that the barrier height an electron sees will effectively vary.[27] In Appendix A, it is estimated that these fluctuations in $V_B$ are as large as 0.1 eV in GaAs for $n_0\sim 10^{19}$ cm$^{-3}$. However, no attempt has yet been made to include these fluctuations in calculations of tunneling currents.

## III. THEORY OF TUNNELING

The calculations of the tunneling currents presented in CDMT were done by some elaborate computer programs. This was necessary because rather exact expressions for the tunneling current were derived and evaluated. The exact asymptotic solutions of the electron's wave function in a parabolic potential were used in the tunneling probabilities, and the angular integrals over perpendicular wave vector were included. This method is cumbersome and cannot be applied to the variety of potentials and effects which will be discussed below. The WKBJ method, however, provides approximate solutions of sufficient accuracy when

[25] E. O. Kane, Phys. Rev. **131**, 79 (1963).

[26] B. I. Halperin and M. Lax, Phys. Rev. **148**, 722 (1966); J. Zittartz and J. S. Langer, *ibid.* **148**, 741 (1966).

[27] D. G. Dow, Proc. IRE **49**, 837 (1961); R. L. Longini, IRE Trans. **ED-9**, 88 (1962).

applied in the form

$$I=\beta\int_{E_1}^{E_2} dE\, E^{1/2}\exp\left[-2\int_{z'}^{z''} dzk(z,E)\right]. \quad (3.1)$$

In this expression, $E$ is the energy of the electron in the semiconductor as measured from the bottom of the conduction band. The integrand contains a density-of-states term $E^{1/2}$. The existence of this factor can be deduced directly from (1) and (9) of CDMT; it is required in order to obtain analytic and numerical correspondence between the WKBJ method and the exact solution of CDMT. We note that tunneling currents evaluated by matching wave functions always show a tunneling probability, proportional to the density of states at low wave vector.[23,28,29] The failure of the WKBJ solution to have this feature implies that WKBJ matching is incorrect for low wave vector. Calculations of the tunneling current and incremental resistance were made for the case of $n$-type Ge. The results from the exact solution of CDMT and the approximate solutions of the WKBJ method using (3.1) were in agreement. To provide an additional justification for our use of the term, we present in Appendix C a discussion of the range of validity of (3.1). The value of $\beta$ varies little with applied voltage, and may be regarded as a constant for the calculations of present interest.

Theory and experiment are compared by plotting the calculated and measured dependence of the incremental resistance $dV/dI$ on applied voltage $V$ in semilogarithmic coordinates. In this way comparisons are made on a relative basis over several orders of magnitude in range of resistance.

We now consider the evaluation of the WKBJ exponent (3.1). For an electron tunneling through a simple potential, one uses

$$k(z)=\left\{\frac{2m}{\hbar^2}[V(z)-E]\right\}^{1/2}. \quad (3.2)$$

The potentials $V(z)$ are those described in the previous section. This form is often quite inaccurate for electrons which tunnel into the forbidden gap of a semiconductor. An electron in the forbidden energy gap is a mixture of valence and conduction-electron states. In a $p$-$n$ junction, the electron tunnels completely from a conduction to a valence band. In a WKBJ classical approximation, this transition takes place smoothly along a trajectory in $k$ space which can be calculated in the effective-mass approximation. These considerations are important in metal-semiconductor tunneling if the electron must penetrate significantly through the forbidden gap. The important ratio is $V_B/E_G$, where $V_B$ is the barrier height, and $E_G$ is the energy gap. For $V_B/E_G>\frac{1}{2}$, the mixing of conduction and valence-band states in the energy gap is important.

The trajectory through the forbidden gap can be calculated easily by assuming a two-band model. Since the effective mass is small, we use Franz's[10,21] expression for the kinetic energy

$$E_{\mathrm{K.E.}}=[E_G^2/4+E_G\hbar^2k^2/2m]^{1/2}-E_G/2\,,$$

rather than Kane's[11] more accurate form. This gives for the $k$ trajectory

$$k(z)=\left\{\frac{2m}{\hbar^2E_G}[V(z)-E][E_G+E-V(z)]\right\}^{1/2}. \quad (3.3)$$

In this expression, the classical turning points of the electron in the conduction and valence band are $V(z)$ and $V(z)-E_G$, respectively.

The WKBJ integrals for the two-band expression (3.3) will be discussed for the parabolic potential $V_p'$ in (2.6). The integrals for the one-band model (3.1), and with the potentials discussed above, are given in Appendix B. It is convenient to introduce

$$E_0=\left[\frac{\pi e^2n_0\hbar^2}{m\epsilon_0}\right]^{1/2}$$

because this factor arises at large forward biases where the current is exponential in voltage, i.e., $I\sim\exp(V/E_0)$ for $V\gg 0$. The tunneling mass, rather than the density-of-state mass, should be used in calculating $E_0$. Energies are normalized with respect to the Fermi energy, viz.,

$$\alpha=(V_B-V+\mu_F)/\mu_F\,,$$
$$\epsilon=E/\mu_F\,,$$
$$C=\mu_F/E_0\,,$$
$$\lambda=E_G/\mu_F\,.$$

Then, using (3.3) and the parabolic potential $V_p'$ in (2.6), twice the WKBJ integral is

$$W=\frac{2}{3}\frac{C}{p}\left\{(\lambda+2\epsilon)E(\chi,p)-2\epsilon F(\chi,p)+(\alpha-\lambda-2\epsilon)\left[\frac{\alpha-\epsilon}{\alpha}\left(\frac{\lambda+\epsilon-\alpha}{\lambda+\epsilon}\right)\right]^{1/2}\right\},$$
$$p=[\lambda/(\lambda+\epsilon)]^{1/2}, \quad (3.4)$$
$$\sin\chi=\left[\frac{\lambda+\epsilon}{\lambda}\left(\frac{\alpha-\epsilon}{\alpha}\right)\right]^{1/2},$$

where $E$ and $F$ are incomplete elliptic integrals. This expression is related to the results of Butcher, Hulbert, and Hulme[12] for asymmetric $p$-$n$ diodes of InSb. They also assumed a parabolic potential and used a two-band model to evaluate their trajectory through the forbidden gap. Since their electrons were tunneling entirely through the gap, from the conduction to the valence

[28] W. A. Harrison, Phys. Rev. **123**, 85 (1961).
[29] R. T. Shuey, Phys. Rev. **137**, A1268 (1965).

band, their limits of integration were the two turning points and the results were expressed in terms of complete elliptic integrals. This corresponds to setting $\alpha=\lambda+\epsilon$ and $\chi=\pi/2$ in the above expression. In metal-semiconductor junctions, the incomplete elliptic integrals are obtained since the electron encounters the metallic surface before being allowed to complete its trajectory through the forbidden gap.

The current integral (3.1), with the WKBJ exponent (3.4), describes quite well the tunneling in $n$-type Ge and $n$-type GaAs. The incremental resistance characteristics of these two materials are quite different.

In $n$-type Ge, CDMT showed that the incremental resistance should peak at a bias equal to the Fermi degeneracy, and this observation agrees with the experimental measurements. The maximum in the background resistance, which occurs at biases equal to the Fermi degeneracy, merely reflects the critical point in the density of states which occurs at bottom of the parabolic conduction band. Since $\mu_F/E_0<1$, electrons at the bottom of the band can tunnel nearly as easily as those at the Fermi energy, and hence the critical point is observed. These features are also predicted by the above current integral (3.1) with (3.4). It is not really necessary to use the two band model for $n$-type Ge: since $V_B/E_G=0.25$, very little band mixing occurs in the forbidden-gap trajectory, and it is equally valid to use the one-band model of CDMT. An extended comparison of the one-band and two-band results for $n$-type Ge is provided in Appendix II. There it is also demonstrated that it is not necessary to include the exponential nature of the band edge (2.5)—the simple parabolic potential (2.6) is adequate for most analyses.

In $n$-type GaAs, as is shown below, the incremental resistance characteristics are quite different than in $n$-type Ge. Yet this case is also well described by the above current integrals. The differences between these two materials are twofold. First of all, in $n$-type GaAs the ratio $\mu_F/E_0>1$, and the electrons at the bottom of the conduction band have a negligible tunneling probability compared to those at the Fermi energy. Hence, one does not see the density-of-sates critical point at the bottom of the band, and the incremental resistance does not peak at a bias equal to the Fermi degeneracy. Secondly, $V_B/E_G=0.6$, and band mixing is important in the forbidden gap. Here it is essential to use the two-band model WKBJ integral (3.4) to predict the tunneling characteristics.

Thus, the above current integral successfully predicts the quite different incremental resistance measurements of $n$-type Ge and $n$-type GaAs. The difference between the tunneling characteristics for these two materials simply arises from the different parameters specifying each case.

## IV. EXPERIMENTAL CONSIDERATIONS

The samples employed in this investigation are, in general terms, diodes. Of primary interest are their electrical characteristics expressed in terms of the dependence of incremental resistance $dV/dI$ on applied voltage $V$. To provide a sufficient description of these samples it is necessary to provide measurement of impurity type and concentration, and to describe the fabrication procedure. Further, it is necessary to show that the measured dependence of capacitance on applied voltage is consistent with assumed features of the model.

Briefly, the fabrication procedure consists of mounting the semiconductor on a header, preparing the surface, and applying the metallic element. The parent crystals were oriented and sawed on {100} planes to produce slices. These were subsequently lapped, multiply ruled with a diamond stylus and broken. In this manner cubes with two lapped and four cleaved faces were fashioned. These were mounted on Au alloy plated TO-18 headers by eutectic solution at 500°C. In the mounting, a cleaved {100} face was positioned to receive the metallic contact. The Au plating contained Sn or Zn in the cases of $n$- and $p$-type GaAs, respectively. The quality of the alloyed contacts was assessed electrically on control devices possessing two such contacts. They proved to be entirely satisfactory. The GaAs was chemically polished in 3:1 $HNO_3$:HCl during which damage from the cleaving was removed and a brightly polished surface was developed. The entire assembly was then electroplated with Au from a cyanide bath to form the Schottky barrier. A contact wire was attached to this surface. Thermocompression bonding with a Au wire of small diameter proved to be most convenient. In this, a temperature below 200°C was used. The plated gold not protected by the masking of the bond was anodically removed in $H_2SO_4$.

The inherently low values of resistance obtained initially were adjusted upward over a limited range by reducing the area with chemical or anodic etching. However, as the useful upper limit is approached, geometry favors a more rapid increase in parasitic series resistance than decrease in barrier resistance. The upper limit of impurity density for which meaningful data can be measured on samples fabricated by the method described was limited by this effect. Anodic etching in 25% NaOH was employed except for the most pure $n$-type GaAs which was chemically etched in 25% NaOH:$H_2O_2$ 5:1.

The technique for obtaining the electrical characteristic is a familiar one and need be described only in brief detail. The incremental resistance $dV/dI$ was measured by applying a small alternating current to the diode and detecting the voltage developed synchronously. Bias was applied by quasistatically sweeping an added current component. The voltages developed were recorded continuously on an $X$-$Y$ plot.

As a matter of secondary importance, the depen-

dences of diode capacitance on applied voltage at 77°K were measured. In principle, the barrier height $V_B$, corroboration of the assumption of uniform impurity distribution, and the density of impurities $n_0$, can be obtained from analysis of these measurements. Practical difficulties, however, reduce the effectiveness of the method.

A fitting of the measured dependence of the capacitance to

$$\frac{C}{A}=\left[\frac{e\epsilon_0}{2\pi n_0(V_B-V+\frac{3}{5}\mu_F)}\right]^{1/2} \tag{4.1}$$

over the accessible range of applied bias $V$ resulted typically in errors less than 1%. The scatter in values determined for height $V_B$ and impurity density $n_0$ was on the order of $\pm5$ and $\pm10\%$, respectively. In the case of $V_B$, this can be understood on the basis of the extrapolation

$$\lim_{C^{-2}\to 0} V=V_B+\tfrac{3}{5}\mu_F. \tag{4.2}$$

For $n_0$, errors in determining the area $A$ are most significant. To measure this, the diodes were destroyed, micrographs were made, and the area taken with a planimeter.

This method is not regarded as being capable of yielding accurate values for $V_B$ and $n_0$ directly. However, the results are important in corroborating essential features in the assumed model. It was consistently observed that:

(1) The measured dependence is that which would result from a uniform distribution of impurities.

(2) The values of $n_0$ measured scatter about the value deduced from Hall-effect data.

(3) The measured values of $V_B$ scatter about the accepted values.[9]

Impurity type and density on samples for which characteristic dependences are presented in subsequent sections can be found in Table I. Corresponding values for the Fermi energy $\mu_F$ are also shown. In calculating these the density-of-states effective mass values of 0.072 for $n$-type GaAs was used. The effect of departure from parabolicity for $n$-type GaAs was approximated by

$$\mu_{F0}=\hbar^2(3\pi^2 n_0)^{2/3}/2m_0 \tag{4.3a}$$

and

$$\mu_F=\mu_{F0}(1-\mu_{F0}/E_G). \tag{4.3b}$$

The accepted value $E_G=1.52$ eV was employed.[7] It is evident, however, that the sum of the barrier heights taken is not equal to this value.

## V. EXPERIMENTAL RESULTS

### A. $p$-Type GaAs

Typical measurements of incremental resistance is given in Fig. 2 for three concentrations of $p$-type GaAs on an approximately linear scale. This allows the structure at zero bias and $-36.4$ meV to be observed on the scale which is customary. The structure at $-36.4$ meV is related to the LO phonon at this energy.[30,13] Since GaAs is weakly polar, this is unquestionably a polaron effect, similar to those observed by Hall *et al.*[13] in $p$-$n$ diodes. These polaron effects will be discussed in Sec. VII.

TABLE I. Impurity type, density, and estimated Fermi degeneracy for the Au-GaAs samples for which results are presented. Also shown are the number of samples $N$ of like construction and similar characteristics. The bias at which the maxima occur in the dependence of $dV/dI$ on applied voltage $V$ is shown as $V_{\max}$ for the $p$-type samples.

| Sample number | Impurity Type | Impurity $n_0$(cm$^{-3}$) | Fermi degeneracy $\mu_F$(eV) | Bias at maxima $V_{\max}(V)$ | Number of samples $N$ |
|---|---|---|---|---|---|
| B2312, B2313, 2332, 2341, 2342 | $n$ | $1.79\times10^{18}$ | 0.0712 | | 15 |
| 2351, 2352 | $n$ | $3.72\times10^{18}$ | 0.12 | | 6 |
| 2003 | $n$ | $4.7\times10^{18}$ | 0.129 | | 4 |
| 2020, 2021, 2022, 2023 | $n$ | $1.0\times10^{19}$ | 0.199 | | 4 |
| B2491, B2493, E2493 | $p$ | $5.4\times10^{18}$ | | $-0.03$ | 7 |
| 2035 | $p$ | $9.9\times10^{18}$ | | $-0.04$ | 6 |
| B2562 | $p$ | $3.6\times10^{19}$ | | $-0.06$ | 8 |

Figure 3 shows the data for $n_0=5.4\times10^{18}$ and $9.9\times10^{18}$ cm$^{-3}$ on a $\ln(dV/dI)$ scale. The data at both concentrations fit very well the theory of CDMT which was developed for $n$-type Ge. This theory is valid for $V_B/E_G<\frac{1}{2}$ and $\mu_F/E_0<1$, and both of these conditions are satisfied for $p$-type GaAs. The three characteristics predicted by this theory are (1) the background peak in $dV/dI$ occurs at the biases equal to Fermi degeneracy, (2) the curve of $\ln dV/dI$ is linear in $V$ above this maximum, and (3) the plot of $\ln dV/dI$ is concave upward for biases below the maximum. The $p$-type GaAs data have the last two characteristics if one recalls that the sign of the bias is reversed in listing these characteristics for $p$-type data. Indeed, the data in Fig. 3 agree with the theoretical calculations of CDMT even better than the data for $n$-type Ge.

At first it was thought that characteristic (1) could be applied to obtain an estimate of the Fermi degeneracy of $p$-type GaAs. This would provide a direct measurement of the density-of-states mass. This interpretation is incorrect because of the important effect

[30] S. J. Fray, F. A. Johnson, J. E. Quarrington, and N. Williams, Proc. Phys. Soc. (London) 77, 215 (1961).

of impurity bands in $p$-type materials. This band penetrates significantly into the forbidden gap because of the heavy-hole mass. The acceptor binding energy in GaAs is about 0.030 eV.[31–34] The incremental resistance

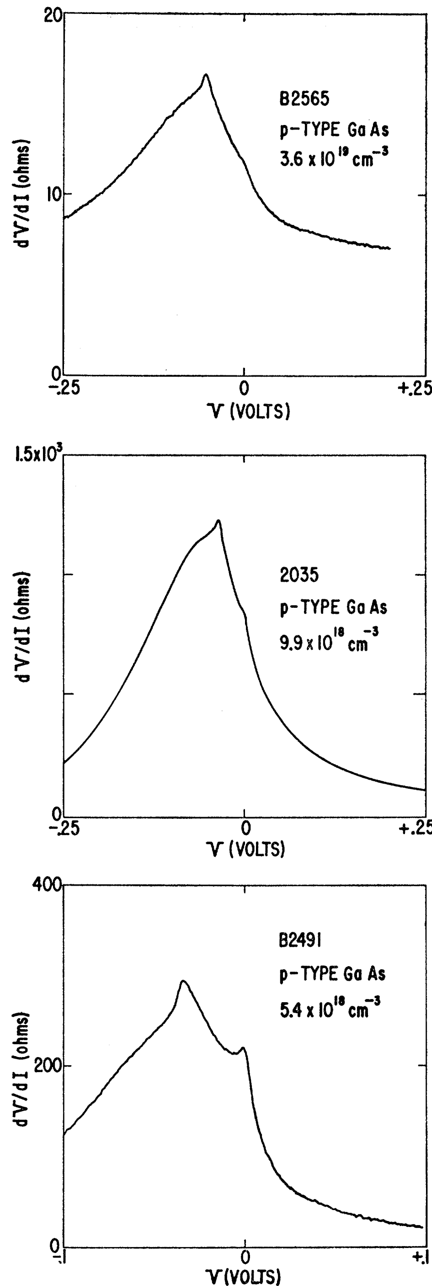


FIG. 2. Examples of the observed dependence of incremental resistance $dV/dI$ on applied voltage $V$ for three samples of $p$-type GaAs. Of interest is the structure at $-0.0364$ eV and at zero bias. There is a systematic shift of the broad maxima in the background dependence toward more negative values with increasing impurity density.

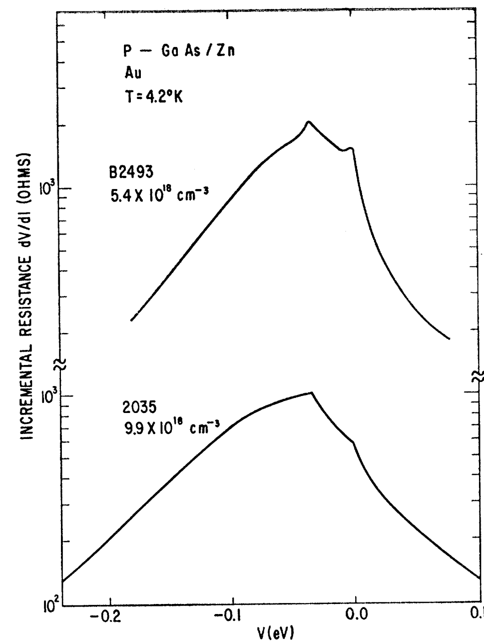


FIG. 3. The incremental resistance for $p$-type GaAs at two different concentrations. This semilogarithmic plot shows that the resistance has the form $\exp(V+V_0)/E_0$ for negative $V$, in agreement with the predictions of Ref. 3.

measurements between $V=0$ and $V=0.10$ eV are affected by the presence of the impurity band. The theory of CDMT, and also the formalism of Sec. III, only describe the measurement outside of this voltage range.

A method is presented in Ref. 8 whereby this $p$-type GaAs data can be analyzed to provide a measurement of the density of states. These results show the presence of the impurity band. An estimate of the impurity band width may be obtained from Fig. 3. In Ref. 8, it is shown that the impurity band meets the parabolic conduction band near the point $V=0$. The lower limit of the impurity band is where the linear behavior for $V<0$ begins, $\log_{10}dI/dV \propto V/E_0$. These bandwidths appear consistent with those observed by Cusano[34] and Pankove[35] in radiative recombination experiments in $p$-type GaAs.

### B. $n$-Type GaAs

It was remarked above that $n$-GaAs is expected to behave differently than the cases previously considered. The background resistance should no longer peak at biases equal to the Fermi energy because electrons at the bottom of the band have too small a tunneling

[31] G. Lucovsky and C. J. Repper, Appl. Phys. Letters 3, 71 (1963).

[32] M. I. Nathan and G. Burns, Appl. Phys. Letters 1, 89 (1962).

[33] J. I. Pankove, Phys. Rev. 140, A2059 (1965); Proceedings of the International Conference on Semiconductors, Kyoto, 1966, J. Phys. Soc. Japan Suppl. 21 (1966).

[34] D. A. Cusano, Solid State Commun. 2, 353 (1964); Appl. Phys. Letters 7, 151 (1965).

[35] This result differs from Padovani and Stratton by the $3/5\mu_F$ factor, which is obtained by including the correct exponential character of the band edge. Since $\mu_F$ is very small compared to $V_B-V$, this factor makes little difference in practice.

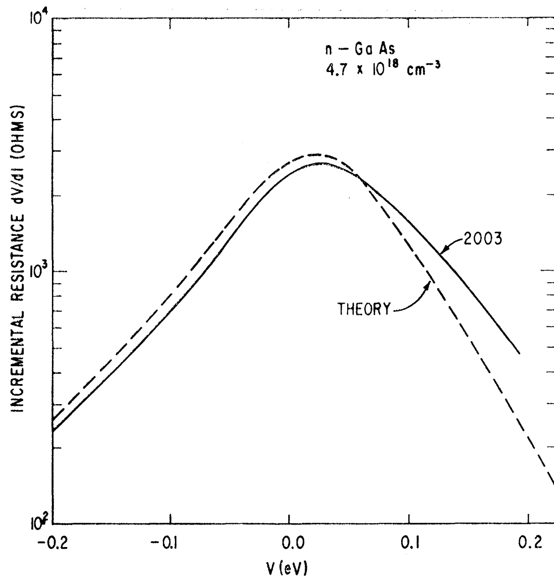


FIG. 4. A comparison of the experimental (solid line) and theoretical (dashed line) incremental resistance of $n$-type GaAs with $n=4.7\times10^{18}$ cm$^{-3}$. The theoretical curve was calculated using the WKBJ integral $W$ in (3.4) for the two-band model. The magnitude of the calculated resistance was adjusted to the experimental value. The shape of the theoretical curve agrees quite well with the experimental result for reverse bias, but the theoretical resistance falls more steeply at forward bias. There are no adjustable parameters in the calculation, since $m=0.072$, $\epsilon_0=13$, $V_B=0.92$ eV, and $E_G=1.52$ eV have all been measured previously.

probability. And since $V_B/E_G=0.6$, the band mixing in the forbidden gap is important.

Incremental resistance measurements for $n$-GaAs are shown in Figs. 4 and 5. In Fig. 5(b), the data are plotted on an expanded linear scale, so that the weak anomalies at zero bias and $\pm\hbar\omega_0$ can be observed. Figure 5(a) shows data from four experimental samples plotted on a semilogarithmic scale. They all have the same voltage dependence, differing only in magnitude. In the design of this experiment, a varying set of areas, hence magnitudes, was deliberate. The scatter among the measured incremental resistance, however, for nominally equal areas, occurs at every concentration measured, and is on the order of a factor of 2. Also included in Fig. 5(a) is the theoretical incremental resistance calculated using (3.1) and (3.4). The theoretical curve agrees with experimental data in shape at reverse but not at forward biases. There are no adjustable parameters in the theoretical calculations. Note that here the resistance maxima occur at biases much less than the estimated Fermi energy of 0.20 eV.

The agreement between theory and experiment is better in the more lightly doped samples, as is shown in Fig. 4. Again the disagreement occurs at forward bias but not at reverse bias. If one did not include band mixing in the theoretical calculation, but used the one-band models of Appendix II for the WKBJ exponents, the calculated curve would have a smooth maximum at zero bias. Thus, the maximum in the incremental resistance appears at forward biases because of the voltage dependence of the band mixing in the forbidden gap. The data for $n$-type GaAs is characterized in an entirely different way than $p$-type GaAs or $n$-type Ge.

## VI. THE DISPERSION RELATION

The effect of dispersion in states of the forbidden gap on the tunneling characteristics in $n$-type GaAs has been demonstrated in Sec. V. Conversely, a relation can be obtained for this dispersion in terms of the

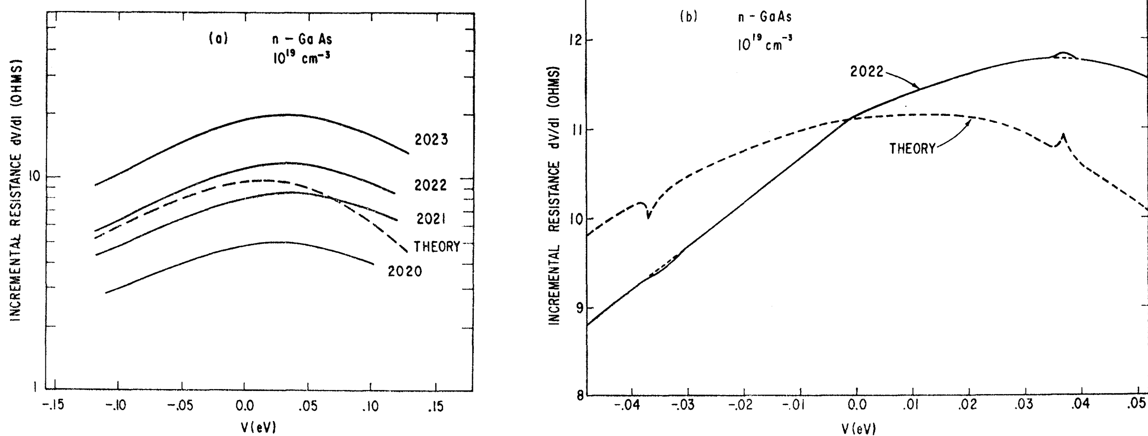


FIG. 5. A comparison of the experimental (solid lines) and theoretical (dashed lines) incremental resistance of $n$-type GaAs with $n=1.0\times10^{19}$ cm$^{-3}$. The four experimental samples in (a) have different magnitudes of resistance because of deliberate differences in junction area. The theoretical curve has the correct shape at reverse but not at forward bias. The same data are shown in (b) on a larger scale, where the weak zero bias and polaron anomalies are apparent. The background conductance (dotted line) is sketched in at the polaron anomalies at $V=\pm\hbar\omega_0$. The theoretical shows the calculated polaron anomalies described in Sec. VII. Introducing broadening into the theoretical shapes would round off the logarithmic singularities into better agreement with the observed structure.

observed dependences. At large forward biases in $n$-type GaAs junctions, the limits of integration on the current integral (3.1) are $E_1=0$, $E_2=\mu_F$. The electrons at the Fermi energy $E=\mu_F$ have the highest tunneling probability. The tunneling characteristics can be estimated by just considering the electrons at the Fermi energy:

$$I=\beta' \exp\left[-2\int_0^{z0} dz k(z,\mu_F)\right]. \quad (6.1)$$

Electrons tunneling from the Fermi energy see the parabolic potential $V_p$ in (2.4a).

From the relation

$$E=E_{\mathrm{K.E.}}+V(z),$$

we see that $k(z,E)$ depends just on $z$ and $E$ through the form $k(V(z)-E)$. Thus set

$$\eta=V(z)-E$$

and at $E=\mu_F$, the above integral becomes

$$\ln I=\ln\beta'-\left(\frac{\epsilon_0}{2\pi n_0 e^2}\right)^{1/2}\int_0^{V_B-V}\frac{d\eta k(\eta)}{(\eta+\frac{3}{5}\mu_F)^{1/2}}.$$

The factor of $\frac{3}{5}$ came from using the correct potential (2.4). If we ignore the weak voltage dependence of $\beta'$, then $V$ only appears in the integration limit. Thus,

$$\frac{d}{dV}\ln I=\left(\frac{\epsilon_0}{2\pi n_0 e^2}\right)^{1/2} k(V_B-V)(V_B-V+\tfrac{3}{5}\mu_F)^{-1/2}.$$

Rearranging this result gives the formula of Padovani and Stratton[4,35]:

$$k^2(V_B-V)=\frac{2\pi n_0 e^2}{\epsilon_0}(V_B-V+\tfrac{3}{5}\mu_F)\left(\frac{d}{dV}\ln I\right)^2. \quad (6.2)$$

This shows that the dispersion relation $k^2(E<0)$ can be obtained in the forbidden gap by experimentally measuring $d\ln I/dV$.

The resulting expression for $k^2(E)$, which is valid for both $n$- and $p$-type GaAs, must be regarded as approximate. The main error in the derivations is from the use of (6.1) instead of the integral (3.1). The extent of this error can be seen by inspection of Fig. 6. Values for $d\ln I/dV$ were calculated numerically from (3.1) for several values of $n_0$. Then, this is related to the dispersion by (6.2) in the same manner as indicated for the reduction of experimental measurements. The dispersion (3.3) employed in the integral (3.1) is also shown for purposes of comparison. An error of about 10% in the value of $k^2$ is seen to result. Padovani and Stratton indicate that the image charge forces will tend to raise the value of $k^2$.

The technique of measuring the dependence of $d\ln I/dV$ on applied voltage is particularly valuable and deserves a brief description. A small alternating voltage and a quasistatically swept voltage are applied

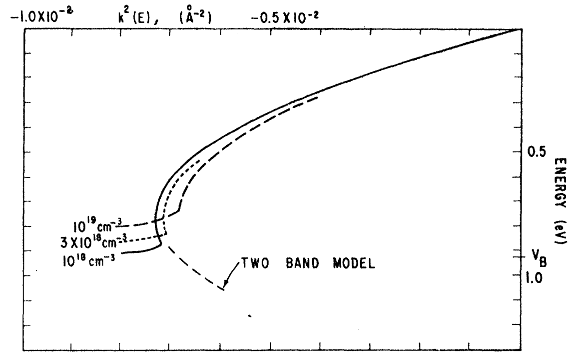


FIG. 6. Calculated $k^2(E)$ curves for different concentrations $n_0$ of impurities. The tunneling current was evaluated using (3.4) in (3.1), and the calculated current was reduced using (6.2). The resulting value for $k^2$ is shown to depend upon concentration. This apparent dependence arises from just taking electrons at the Fermi energy in (6.1) rather than using the integral (3.1) over the electronic states.

to the diode by an operational amplifier of low output impedance. The resulting output current is directly coupled into an operational amplifier which has both a low input impedance and a logarithmic transimpedance. Synchronous detection of the alternating component of the output produces the desired function. The useful range of currents in the particular instrument employed was 30 nA to 3 mA for a precision better than 4%. The lower limit was set by offset current and the upper limit was set by departure from logarithmic response due to series resistance in the feedback element, i.e., a 2N930 transistor. The implementation follows standard practices. A complete description of the equipment and a discussion of the general aspects of the measurement, much of which is of temporal nature, is to be published separately.

Examples of the logarithmic characteristics obtained in this manner are shown in Fig. 7 for $n$- and $p$-type

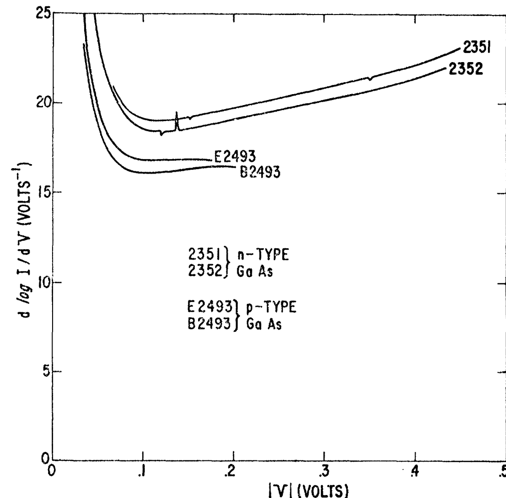


FIG. 7. Examples of forward bias characteristics measured directly as $d\ln I/dV$ for $n$- and $p$-type GaAs.

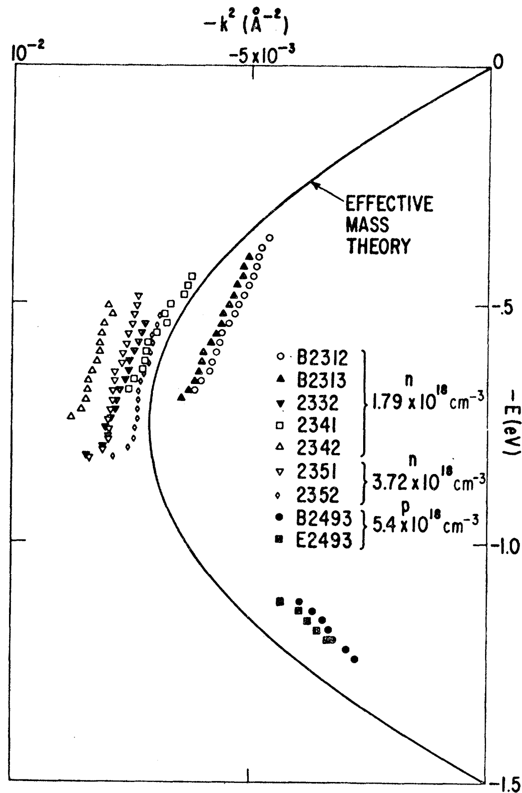


FIG. 8. Experimental determination of dispersion in states of the forbidden energy gap in GaAs. Data for both $n$- and $p$-type GaAs are shown. Also shown is the dispersion predicted by effective-mass theory in the two-band model (Ref. 10).

GaAs, respectively. The singular behavior at small applied voltage occurs for currents well above the lower limit set by the instrumentation and is expected on the basis of the preceding discussion of errors in the theoretical treatment. The upper boundary is fixed either by the limitations in the instrumentation or by the effect of parasitic series resistance in the sample.

Results for several samples from a range of impurity concentrations of both $n$- and $p$-type GaAs are shown in Fig. 8. The values for barrier height $V_B$ and impurity density $n_0$ employed in the reduction were discussed in Sec. IV and presented in Table I, respectively. The scatter observed can be attributed both to uncertainties in specification of these parameters and also to variations in the fabrication. Since the $p$-type data fall consistently above the effective-mass curves, this suggests that the light hole mass may even be smaller than predicted from the two-band model.

The effect of excess heating in the fabrication proved detrimental. Successively higher temperatures produces correspondingly lower values of $k^2$. Further, pronounced structure was observed in these data (not shown). No change other than occasional loss of mechanical integrity was observed below a fabrication temperature of 200°C.

The values for the dispersion as measured are consistent with the dependence predicted by (3.3) from the effective mass formalism. In no sample were values of $k^2$ observed as large in magnitude as those reported by Padovani and Stratton.[4]

## VII. POLARON SINGULARITIES

The incremental resistance measurements show structure at $V=\pm\hbar\omega_0=\pm36.4$ meV. This is caused by the electron's interaction with LO phonons at that frequency.[30,13] In $n$-type GaAs, the structure is observed at both forward and reverse bias, although it appears less broadened at forward bias, as in Fig. 5(b). For $p$-type GaAs, strong structure is observed at reverse bias $V=-\hbar\omega_0$; at forward bias the observed structure is so slight that it is not even apparent on Fig. 2. Thus, the anomaly appears with a strength which is asymmetric across the Fermi energy. The strong side corresponds to effects which occur below the Fermi energy of the respective electron or hole plasma. Polaron effects, corresponding to tunneling thresholds, were first observed in GaAs $p$-$n$ junctions by Hall *et al.*[13] There they also corresponded to effects which were $\hbar\omega_0$ beneath the Fermi energy of the electron and hole plasma.

Calculations on polaron effects in degenerate semiconductors predicted that such anomalies should exist.[19,20] In polar semiconductors, the low-temperature electronic dispersion relations are altered for energies $\pm\hbar\omega_0$ away from the Fermi energy. This causes the density of states to have a logarithmic singularity at energies $E=\mu_F\pm\hbar\omega_0$. These calculations predict that the logarithmic singularity should have nearly equal strength above and below the Fermi energy, especially when $\mu_F\gg\hbar\omega_0$. This agrees with the $n$-type data, although it is not understood why the structure above the Fermi energy (appearing at $V=-\hbar\omega_0$) is broadened more. The $p$-type data are even more inexplicable since the polaron structure appears very strongly at $V=-\hbar\omega_0$ and very weakly at $+\hbar\omega_0$. The calculations predict only a slight asymmetry in the strength of the logarithmic singularity below and above the Fermi energy even for $\mu_F\gtrsim\hbar\omega_0$. A possible explanation is to note that the mean free path is longer for electrons near the top of the valence band. This is because the energy width $\Gamma$ is proportional to the density of states $\Gamma\sim E^{1/2}$ for the dominant damping mechanism of impurity scattering. This makes $\Gamma$ smaller for the singularity at $E=\mu_F-\hbar\omega_0$, than at $E=\mu_F+\hbar\omega_0$ (when $\mu_F\simeq\hbar\omega_0$), which may explain why the structure is more easily observed at $V=-\hbar\omega_0$.

Some calculations were made in order to compare the predicted polaron anomalies with those observed experimentally. It was shown previously[20] that the important structure arises from the term in the elec-

tronic self-energy denoted $\Sigma_F$:

$$\mathrm{Re}\Sigma_F(p,E)=\frac{4\pi\alpha\omega_0^{3/2}}{(2m)^{1/2}}\int\frac{d^3q}{(2\pi)^3}\frac{n_F(\mathbf{p}+\mathbf{q})}{q^2\epsilon(q)^2}\times\left[\frac{1}{E+\omega_0-\epsilon_{\mathbf{p}+\mathbf{q}}}-\frac{1}{E-\omega_0-\epsilon_{\mathbf{p}+\mathbf{q}}}\right].$$

The Fermi-Thomas approximation is used for the dielectric function $\epsilon=1+k_s^2/q^2$. This self-energy predicts a logarithmic singularity and this part of $\mathrm{Re}\Sigma_F$ is given by

$$\mathrm{Re}\Sigma_F(p,E)=g(p)\ln\left|\frac{E-\omega_0-\mu_F}{E+\omega_0-\mu_F}\right|,$$

$$g(p)=\frac{\alpha}{4\pi}\frac{(\hbar\omega_0)^{3/2}}{(\mu_F)^{1/2}}\left\{\ln\frac{(p+p_F)^2+k_s^2}{(p-p_F)^2+k_s^2}+\frac{k_s^2}{(p+p_F)^2+k_s^2}-\frac{k_s^2}{(p+p_F)^2+k_s^2}\right\}.$$

The function $g$, always positive, depends only weakly upon $p$ for $\epsilon_p\leq 4\mu_F$. Thus, it can be conveniently approximated by its value at $p=0$:

$$g_0=\frac{\alpha}{\pi}\frac{(\hbar\omega_0)^{3/2}}{(\mu_F)^{1/2}}\frac{1}{(1+k_s^2/p_F^2)^2}.$$

Also, when solving the electron's dispersion relation $E(p)$,

$$E=\epsilon_p+\mathrm{Re}\Sigma_F(p,E),$$

the easiest way to proceed is to solve for $p(E)$:

$$\epsilon_p\approx E-g_0\ln\left|\frac{E-\omega_0-\mu_F}{E+\omega_0-\mu_F}\right|\equiv\mathcal{E}(E).$$

For the WKBJ calculations, this expression can be generalized to include potentials $V(z)$ and band mixing by using the form

$$E_{\mathrm{K.E.}}(k)+V(z)=\mathcal{E}(E),$$

where $E_{\mathrm{K.E.}}$ is given in (3.3). This shows that polaron effects can be included in tunneling by replacing $E$ in the tunneling integrals by $\mathcal{E}(E)$. This approach can also be justified by using the formalism of Cohen, Falicov, and Phillips[36] and invoking the quasiparticle approximation. Actually, one should add to the density of states a factor of

$$|1+(\partial/\partial\epsilon_p)\,\mathrm{Re}\Sigma_F(p,E)|^{-1}.$$

This factor can be ignored since the structure in the tunneling data is not caused by density-of-states perturbation in the semiconductor. Resistance anomalies due to density-of-states effects would have the logarithmic singularities occurring with the opposite sign as those observed. The anomalies observed in the resistance are caused by changes in the tunneling probability, or WKBJ exponent, wrought by the polaron singularities.

In the conduction band the polaron constant is $\alpha_c=0.06$.[13] For $n_0=10^{19}$ cm$^{-3}$, GaAs has $\mu_F=0.2$ eV and $g_0=0.2$ meV. The constant $g_0$ is very small, yet it is large enough to explain the observed anomalies. Figure 5(b) shows a comparison of the theoretical and experimental incremental resistance for $n_0=10^{19}$ cm$^{-3}$. The calculated anomalies are of the same size as those observed in the data. No theoretical calculations were made for comparison with the $p$-type data. Since $\mu_F\approx\hbar\omega_0$ for these samples, the polaron singularities occur in the region of band tailing. Several features of the polaron effects in valence bands should be mentioned.

Since the polaron scattering mixes the light- and heavy-hole bands, the effective constant $\bar{\alpha}$ for the valence band is the average of the $\alpha$'s for the light- and heavy-hole band[37]; roughly $\bar{\alpha}=\frac{3}{2}\alpha_c$. For $p$-type data, when $\mu_F=\hbar\omega_0$, then $g=0.7$ meV which is larger than for $n$-type data. This easily explains why the polaron anomaly observed in $p$-type data is significantly larger than that for $n$-type; the important ratio $g/\mu_F$ is 20 times larger here. These estimates are approximate since calculations on $p$-type data are unreliable because the hole plasma is not a high-density electron gas and Fermi-Thomas screening is not really appropriate.

The analysis of polaron effects is simpler in metal-semiconductor junctions than in $p$-$n$ junctions. As shown above, the polaron effects were properly included as alterations in the electron's dispersion relations. In $p$-$n$ junctions, three different polaron effects must be included. Let $\alpha_c$ and $\alpha_v$ refer to the polaron constants for the $n$ and $p$ side of the junction. Then one term is proportional to $\alpha_c$ and represents changes in the conduction-electron's dispersion relation. The second term is $\alpha_v$ and represents changes in the valence-electron's dispersion relation. The third term $\sim(\alpha_c\alpha_v)^{1/2}$ and represents interactions in the junction region. If one views tunneling as the spontaneous creation of electron-hole pairs in the junction, which is an equivalent way of viewing previous formulations,[11] then the third term $\sim(\alpha_c\alpha_v)^{1/2}$ represents electron-hole final-state interactions (via phonons) in the junction. A complete analysis of $p$-$n$ polaron effects would need to include all three of these effects. Also, in $p$-$n$ junction tunneling, the phonon scattering is often necessary to conserve electronic wave vector, which is not needed in the Schottky barrier. Polaron effects in a metal-semiconductor junction are obviously simpler to understand.

[36] M. H. Cohen, L. M. Falicov, and J. C. Phillips, Phys. Rev. Letters 8, 316 (1962).

[37] G. D. Mahan, J. Phys. Chem. Solids 26, 751 (1965).

## VIII. DISCUSSION

In classifying the characteristics of Schottky barriers there are two important parameters. The first is $\mu_F/E_0$, and the resistance peaks at biases equal to $\mu_F$ for values $\mu_F/E_0<1$. The second parameter is $V_B/E_G$, and band mixing becomes important for $V_B/E_G>\frac{1}{2}$. These two parameters define four classes of behavior, of which two have been observed experimentally. The first was $\mu_F/E_0<1$, $V_B/E_G\leq\frac{1}{2}$ ($n$-type Ge and $p$-type GaAs), and the incremental resistance peaks at $V=\mu_F$ except when impurity bands are important. The second case is $\mu_F/E_0\gg1$, $V_B/E_G\geq\frac{1}{2}$ ($n$-type GaAs), and the resistance peaks smoothly at a forward bias independent of $\mu_F$. Calculations have also been done for the other two cases, although they have not been encountered experimentally. The case $\mu_F/E_0<1$, $V_B/E_G\geq\frac{1}{2}$ still peaks at $V=\mu_F$, while the case $\mu_F/E_0\gg1$, $V_B/E_G<\frac{1}{2}$ has a broad maximum at zero bias. In degenerate $n$-type semiconductors which have $\mu_F/E_0\leq1$, one can thereby directly measure the Fermi energy by the position of the resistance maximum.

It was shown in Sec. III that a theory of tunneling, employing the two-band model, was able to explain all of the observed behavior in these systems. Furthermore, it was shown in Sec. VI that the electrons trajectory in the forbidden gap could be measured. These results were consistent with the two-band model. Thus a self-consistent tunneling theory has been attained which describes these GaAs junctions.

An analysis of the polaron singularities occurring at $V=\hbar\omega_0$ demonstrates that they are explained by the usual precepts of many-body theory. Good agreement between theory and experiment in $n$-type GaAs is obtained by describing the anomalies as alterations in the electron's dispersion relation which affect the tunneling probability via the WKBJ exponents. No anomalies due to plasmon effects were observed, although they are in a suitable frequency range for the lighter doped samples. Raman scattering[38] has shown that this excitation is quite broadened compared to LO phonons, which probably explains why it does not show up in tunneling.

Zero-bias anomalies[13–18] are observed in both $n$- and $p$-type GaAs, although they are much stronger in $p$-type. In the $p$-type data they appear larger in the lower concentration samples. Phenomena similar in appearance have been observed by Wyatt[14] and by Rowell and Chen[16] in metal-oxide junctions. A basic difference is that they observe a conductance maximum while Schottky barriers have a resistance maximum. Logan and Rowell[15] have also observed conductance maxima in heavily doped Si and Ge $p$-$n$ junctions. The conductance maxima have a logarithmic form, and have been explained in terms of Kondo scattering by Appelbaum[17] and Anderson.[18] The resistance maxima observed here are caused by a different mechanism. In Ref. 8 it is shown that the resistance maximum is probably due to structure in the density of states. This structure arises from the details of how the impurity band merges with the parabolic valence band. Since the impurity band is much deeper in $p$-type than in $n$-type GaAs, this explains why the observed anomaly is so much larger in the former material.

[38] A. Mooradian and G. B. Wright, Phys. Rev. Letters 16, 999 (1966).

## ACKNOWLEDGMENTS

We wish to thank T. J. Soltys for making the measurements of the Hall effect and for his advice on technological aspects of sample preparation. Conversation with R. N. Hall, R. T. Shuey, and J. J. Tiemann have been quite helpful.

## APPENDIX A: FLUCTUATIONS IN BARRIER HEIGHT

The fluctuation in the barrier height can be estimated using Klauder's[39] formula for the Markov average of the impurity potential. While in the junction, an electron sees a potential which is the sum of the unscreened Coulomb interactions from the positive impurities and the surface charges. It is convenient to view the surface charges as the image charges of the ions.[2] This model maintains long-range charge neutrality regardless of the fluctuations of the impurity positions, but it provides no insight as to how the surface charges were formed originally.[40] Since the barrier is large at the metal's surface, for simplicity only the images on the metal are considered. For an impurity at $R_j$, and an electron at $z$, the potential is

$$V(\mathbf{R}_j,z)=-\frac{e^2}{\epsilon_0}\left[\frac{1}{|\mathbf{R}_j-\mathbf{z}|}-\frac{1}{|\mathbf{R}_j+\mathbf{z}|}\right].$$

We also make the approximation that the thickness of the junction $z_0$ is independent of the local concentration of impurities. Then Klauder's distribution function can be approximated by a Gaussian

$$P(V_B)=\frac{1}{v(2\pi)^{1/2}}\exp\left[-\frac{(V_B-\bar{V})}{2v^2}\right],$$

where the first two moments are, for $0\leq z\leq z_0$,

$$\bar{V}=n_0\int_{0\leq R_z\leq z_0}d^3RV(R,z)=\frac{2\pi e^2n_0}{\epsilon_0}[(z-z_0)^2-z_0^2],$$

$$v^2=n_0\int_{0\leq R_z\leq z_0}d^3RV(R,z)^2=\frac{2\pi e^4n_0z_0}{\epsilon_0^2}f(z/z_0),$$

and for $0\leq x\leq1$

$$f(x)=2x-(1+x)\ln(1+x)-(1-x)\ln(1-x).$$

[39] J. R. Klauder (unpublished), mentioned in Ref. 25.
[40] V. Heine, Phys. Rev. 138, A1689 (1965).

The function $f(z/z_0)$ has an average value of $f \simeq 0.8$ in the junction. For $n$-type GaAs with $10^{19}$ cm$^{-3}$ impurities, then $z_0 \simeq 100$ Å and $v \simeq 0.1$ eV. A variation in potential barrier of 0.1 eV changes the tunneling characteristics a significant amount, so that these fluctuations are large. Electrons can tunnel more readily at the lower barrier height. Reducing the barrier height makes the junction look more ohmic; so the effect of the fluctuations is to make the resistance less voltage-dependent. This may explain why calculations of the incremental resistance always predict a faster decline of $dV/dI$ with $V$ than observed experimentally. Excessive simplification in this fluctuation model precludes a detailed comparison experiment, e.g., the junction width $z_0$ really depends upon $V_0$ and $V$. Further, it is not clear that band-tailing phenomena can be separated from fluctuations in barrier potentials.

## APPENDIX B: WKBJ INTEGRALS

The WKBJ integrals for the one band model are presented in this Appendix. The WKBJ integrals, and the predicted $dI/dV$ curves for $n$-type Ge, are evaluated for the two junction potentials of Sec. II. These results are compared with similar calculations using the two-band model (3.4). It is shown that all of these methods predict similar effects in $n$-type Ge. Therefore, we reach two conclusions: (1) The one-band model is adequate for describing $n$-type Ge, and it is unnecessary to employ the two-band formalism. This justifies the one-band calculations of CDMT. (2) Including the exponential behavior of the barrier potentials appears to be an unnecessary sophistication. The simple parabolic potential $V_p'$ in (2.6) is adequate for most treatments.

The WKBJ integrals will now be presented for the one-band model (3.2). For the parabolic potential $V_p'$ in (2.6), twice the WKBJ integral is

$$W_1 = C\left\{(\alpha(\alpha-\epsilon))^{1/2} - \epsilon \ln\left[\frac{(\alpha)^{1/2}+(\alpha-\epsilon)^{1/2}}{(\epsilon)^{1/2}}\right]\right\}. \quad \text{(B1)}$$

The notation is defined in Sec. III.

When evaluating the expressions for the parabolic-exponential barrier (2.5), one must distinguish between forward and reverse bias. For reverse bias ($V<0$), the tunneling electrons see just the parabolic part of the potential. Then the WKBJ integral $W_2$ has the same form as (B1), except that $\alpha$ and $\epsilon$ are replaced by

$$\alpha' = \alpha - \tfrac{2}{5},$$
$$\epsilon' = \epsilon - \tfrac{2}{5}.$$

The extra factors of $\frac{2}{5}$ occur because the parabola for this potential ends $\frac{2}{5}\mu_F$ above the bottom of the conduction band. At forward biases ($V>0$), the tunneling electrons see the combination of parabolic and exponential dependence. The WKBJ integrals for the two parts can be added:

$$W_2 = W_{2p} + W_{2e}. \quad \text{(B2)}$$

The parabolic part is

$$W_{2p} = C\left\{(\alpha'(\alpha-\epsilon))^{1/2} - (0.6(1-\epsilon))^{1/2} - \epsilon' \ln\left[\frac{(\alpha')^{1/2}+(\alpha-\epsilon)^{1/2}}{(0.6)^{1/2}+(1-\epsilon)^{1/2}}\right]\right\}$$

and the exponential part is

$$W_{2e} = \frac{4C}{\sqrt{3}}\left[(1-\epsilon)^{1/2} - (\epsilon)^{1/2}\tan^{-1}\left(\frac{1-\epsilon}{\epsilon}\right)^{1/2}\right].$$

At the bottom of the conduction band, $\epsilon \to 0$, these integrals are finite, although the exponential barrier becomes infinitely thick in this limit.

The WKBJ integrals for the parabolic potential $V_p'$ (2.6) and the two band model is given in (3.4). Analytic expressions have also been obtained for the WKBJ integrals using the exponential-parabolic potential for the two-band model. Because they are lengthy and because the exponential behavior does not seem to be an important effect, these expressions are omitted.

The different methods of calculation are compared now for $n$-type Ge with $n = 10^{19}$ cm$^{-3}$. Figure 9 shows

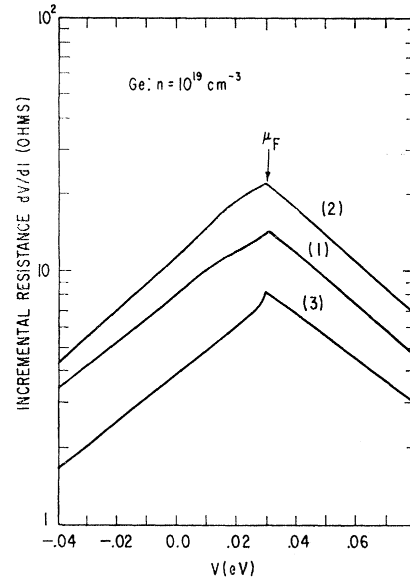


FIG. 9. The incremental resistance calculated for $n$-type Ge using the WKBJ integrals of Sec. III. Curve (1) uses $W_1$ in (B1) for the parabolic potential $V_p'$ in (2.6) and one-band model (3.2); curve (2) uses $W_2$ in (B2) for the parabolic-exponential potential $V_{ep}$ in (2.5) and the one-band model (3.2); curve (3) uses $W$ in (3.4) with the parabolic potential $V_p'$ and the two-band model (3.3). The results are all similar with all curves peaking at biases equal to the Fermi energy $\mu_F = 0.03$ eV. This shows that including the exponential character of the electron's potential is an unnecessary sophistication in evaluating the tunneling characteristics. The parameters used in the calculation were $m = 0.12$, $\epsilon_0 = 16$, $n_0 = 10^{19}$ cm$^{-3}$, $V_B = 0.52$ eV, and $E_G = 2.2$ eV, where 2.2 is the band gap at the zone edge.

the incremental resistance calculated from the three WKBJ forms $W_1$, $W_2$, and $W$ in (3.4). Curve (1) is the parabolic potential using $W_1$, (2) is the exponential-parabolic potential $V_{ep}$ result $W_2$, and (3) employs the parabolic potential with the two band model $W$. There is remarkably little difference in the shapes of these three curves. Curve (2) is higher because the potential $V_{ep}$ has a thicker junction than $V_p'$ which raises the resistance. Curve (3) is lower because the magnitude of the decaying wave vector (3.3) always is less than (3.2), so the resistance is less. Since $V_B/E_G=0.52/2.2=0.25$ is small, the shape of curve (3) is similar to the others. This shows that it is unnecessary to use the two band model (3.3) in $n$-type Ge, which justifies the simpler model used in CDMT.

All three curves of Fig. 2 peak at positive biases equal to the Fermi degeneracy $\mu_F=0.030$ eV. The experimental curves have a smoother maximum at the Fermi energy.[5] The experimental smoothness is probably due to the effect of band tailing, which smooths out the discontinuity in the density of states which occurs at the bottom of the conduction band.

The peak in the resistance occurs at the Fermi energy because electrons at the bottom of the band can tunnel almost as readily as those at the Fermi energy. It is in this case when one would expect that it would be important to include the exponential character of the electronic potential. However, the calculations show that, except for increasing the junction thickness, this refinement changes the theoretical predictions little and is unnecessary.

## APPENDIX C: THE DENSITY OF STATES IN TUNNELING

A feature of a WKBJ solution is that, as shown by Harrison,[28] the tunneling probability is independent of the density of states. The WKBJ method is essentially a high-energy approximation and fails near the bottom of the band. The dependence of the tunneling probability on the density of states has been shown quite generally by Shuey[29] for the electrons near the bottom of the band. Further, in the particular case of the Schottky barrier, it will be shown below that the exact solution of CDMT exhibits this dependence. Equation (3.1) is a method devised to extend the validity of the WKBJ solution. To justify this procedure, the deficiencies in the WKBJ approximation are discussed and the form of Eq. (3.1) is deduced from the exact solution of CDMT. As a result of this discussion, the limitations in the range of validity for Eq. (3.1) are obtained in explicit form.

The WKBJ solutions are never correct as $k\to 0$. As an example, in the particular case of an exponential barrier the criterion for validity is readily established. Consider the potential

$$V(x)=(\hbar^2k_0^2/2m)e^{k_cx},$$

where $k_0$ and $k_c$ are parameters which characterize the dependence. Schrödinger's equation for this potential can be solved exactly and the WKBJ solution can be obtained following the procedure described by Heading.[41] If we choose the normalization[28] for the wave function $\psi(x)$ for $x\ll 0$,

$$\psi(x)=(2/L)^{1/2}\cos(kx+\delta),$$

then in the barrier $x\gg 0$ the exact and WKBJ solutions are

$$\psi(x)_{\text{exact}}=\left(\frac{k\sinh(2\pi k/k_c)}{Lk_0}\right)^{1/2}\exp\left\{-\frac{k_cx}{4}-\frac{2k_0}{k_c}\times\exp(k_cx/2)\right\},$$

$$\psi(x)_{\text{WKBJ}}=\left(\frac{k}{2k_0L}\right)^{1/2}\exp\left\{\frac{\pi k}{k_c}-\frac{k_cx}{4}-\frac{2k_0}{k_c}\exp(k_cx/2)\right\}.$$

In the limit of $k/k_c\gg 1$ the two solutions are equal. However, for $k/k_c\ll 1$ the exact solution has $\psi(x)\sim k$ which results in a tunneling probability which is proportional to the density of states. The WKBJ result is explicitly incorrect in this limit.

Examination of the exact solution of CDMT shows that, for the problem of interest, tunneling is proportional to the density of states for electrons with small wave vectors. To justify the use of Eq. (3.1) it is necessary to show equivalence to the exact solutions and further to establish the range of validity for the approximation involved. Let $E$ be the energy of the electron measured with respect to edge of the conduction band. The essential features in the solution of CDMT Eqs. (1) and (9) are retained by letting

$$I=C(V)\int_{E_1}^{E_2}dE\int_0^E dE_\perp(E-E_\perp)^{1/2}\times\exp((E-E_\perp)/E_3). \quad \text{(C1)}$$

These variables are related to those of CDMT by

$$E_0=(\pi e^2n_0\hbar^2/m\epsilon_0)^{1/2},$$
$$E_3=2E_0/\ln(\rho_0^2/2)=2E_0/\ln[(V_B+\mu_s-V)/E_0],$$
$$E_\perp=Ev^2/v_{\max}^2,$$
$$E-E_\perp=2E_0K_{rz}^2.$$

Factors in the integrand (9) of CDMT which vary slowly with respect to energy are ignored, while the additional $V$ dependence of the WKBJ integrals are indicated in the factor $C(V)$. For $E/E_3\gg 1$, the integrand is largest at small $E_\perp$. Hence, Eq. (C1)

---

[41] J. Heading, *An Introduction ot Phase-Integral Methods* (John Wiley & Sons, Inc., New York, 1962).

becomes

$$I = E_3 C(V) \int_{E_1}^{E_2} dE\, E^{1/2} e^{E/E_3}. \tag{C2}$$

The restriction $E/E_3 > 1$ can be written equivalently as

$$E/E_0 > 2/\ln(V_B/E_0). \tag{C3}$$

If electrons of energy $E$ less than set by this inequality are important in the tunneling process then the angular integrals must be included and a $E^{3/2}$ rather than $E^{1/2}$ dependence then applies.

The WKBJ solution for the parabolic barrier is equal to the exact solution of CDMT for

$$E > 4E_0. \tag{C4}$$

This can be seen by rewriting Eq. (9) of CDMT in a form appropriate to this limit and comparing terms with the integral form of Appendix B. For $E > 4E_0$ the tunneling is not proportional to the density of states, and the conclusions of Harrison[28] pertain.

The range in energy over which the integrand in the expression for tunneling must include the density of states factor $E^{1/2}$ is from Eqs. (C3) and (C4)

$$4 > E/E_0 > 2/\ln(V_B/E_0). \tag{C5}$$

For $n$-type GaAs at $n_0 = 10^{19}$ cm$^{-3}$, $E_0 \sim 0.07$ eV and $V_B = 0.92$ eV the range in energy becomes

$$0.28 \text{ eV} > E > 0.07 \text{ eV}. \tag{C6}$$

This is the range which is significant in the tunneling processes of interest.

PHYSICAL REVIEW VOLUME 161, NUMBER 3 15 SEPTEMBER 1967

# Stress Dependence of Photoluminescence in GaAs

R. N. Bhargava and M. I. Nathan
*IBM Watson Research Center, Yorktown Heights, New York*
(Received 28 April 1967)

Photoluminescence in GaAs at $k=0$ under uniaxial stress up to 14 000 kg/cm$^2$ is studied at 2°K. The stress dependence of the coupling between $J=\frac{3}{2}$, $m_j=\pm\frac{1}{2}$ and $J=\frac{1}{2}$, $m_j=\pm\frac{1}{2}$ valence bands is observed. The deformation-potential constants for the valence band and for the acceptor ground state are determined, and the values for the valence band are $a=-8.9$ eV, $b=-1.96$ eV, and $d=-5.4$ eV.

## I. INTRODUCTION

The application of uniaxial stress to a semiconductor shifts the energy extrema. The top of the valence band in GaAs, which is fourfold degenerate at $k=0$ at zero stress, splits into two doubly degenerate components. There will also be changes in the ionization energy of impurity levels. Since the conduction band is nondegenerate, these changes for shallow donor levels are expected to be small compared to energy-gap changes. In contrast, since the valence-band degeneracy is removed, changes in shallow acceptor ionization energies are expected to be comparable to energy-gap changes.[1]

Studies of the stress dependence of the photoluminescent spectra near the energy gap can be used to determine deformation-potential constants. Because of the large stress effect on acceptor levels, the stress dependence of the spectrum can also be used to determine whether or not an acceptor level is involved in a particular transition. Such studies have been carried out on GaAs photoluminescent spectra for stress $\chi$ applied in the $\langle 100\rangle$, $\langle 110\rangle$, and $\langle 111\rangle$ directions at 2°K. Two lines have been studied: line A at 1.511 eV and line B at 1.490 eV. Our results support the hypothesis that line A does not involve an acceptor level but line B does. This is consistent with the results of Leite and Di Giovanni[2] who attributed line B to a donor-acceptor pair transition. At low stresses, the variation in band-gap energy $E_g$ is linear in $\chi$.[3] However, at high stresses, a quadratic dependence of $E_g$ on $\chi$ is expected[4–6] from a stress-induced coupling between the top of the valence band and the deep lying spin-orbit split-off band. Both linear and quadratic terms are then used to obtain the deformation potential constants.

## II. EXPERIMENTAL METHODS AND RESULTS

The arrangement for the photoluminescent measurements has already been described elsewhere.[7] A compressive stress up to 14 000 kg/cm$^2$ on the sample was applied with an apparatus similar to one described by

[1] P. J. Price, Phys. Rev. **124**, 713 (1961).

[2] R. C. C. Leite and A. E. Di Giovanni, Phys. Rev. **153**, 841 (1967).

[3] G. E. Pikus and G. L. Bir, Fiz. Tver. Tela **1**, 1642 (1959) [English transl.: Soviet Phys.—Solid State **1**, 1502 (1959)].

[4] H. Hasegawa, Phys. Rev. **129**, 1029 (1963).

[5] J. C. Hensel and G. Feher, Phys. Rev. **129**, 1041 (1963).

[6] A. P. Smith, M. Cardona, and F. H. Pollak, Bull. Am. Phys. Soc. **12**, 101 (1967).

[7] M. I. Nathan and G. Burns, Phys. Rev. **129**, 125 (1963). A He-Ne laser was used for excitation of the spectra.